Open Ceramics 16 (2023) 100459

Contents lists available at ScienceDirect

Open Ceramics

journal homepage: www.sciencedirect.com/journal/open-ceramics

Mechanochemical synthesis and characterization of strontium substituted apatite for biomedical application

Yuta Otsuka [a,*], Besim Ben-Nissan [b], Hiroshi Kono [a], Tetsuo Sasaki [c,d], Masafumi Kikuchi [a]

[a] Department of Biomaterials Science, Graduate School of Medical and Dental Sciences, Kagoshima University, 8-35-1 Sakuragaoka, Kagoshima, 890-8544, Japan
[b] School of Life Sciences, Faculty of Science, University of Technology Sydney, PO Box 123, Broadway, NSW, 2007, Australia
[c] Graduate School of Medical Photonics, Shizuoka University, Hamamatsu, Shizuoka, 432-8011, Japan
[d] Research Institute of Electronics, Shizuoka University, Hamamatsu, Shizuoka, 432-8011, Japan

ARTICLE INFO

Handling Editor: Jens Guenster

Keywords:
Strontium substituted apatite
Mechanochemical synthesis
Lattice parameters
Terahertz spectroscopy

ABSTRACT

Strontium-substituted apatite has been proposed as a promising material for osteoporosis treatment. Several synthesis methods have been attempted in the past. In this study, we investigated a method known as the mechanochemical synthesis method. Characterization was carried out using different amounts of strontium ions in the hydroxyapatite (HAp) matrix with FT-IR spectral analysis, X-ray diffraction, lattice constant measurements, differential thermal analysis (DTA), terahertz spectroscopy, and investigation of the basic morphology using scanning electron microscopy (SEM), energy dispersive X-ray analysis (EDX). We report that the development and performance of mechanochemical synthetic pathways are more efficient and economical than other substituted apatite formation methods and are useful in the biomedical field to produce calcium phosphate-based clinical materials. The FTIR spectra, terahertz spectra, and XRD analysis results revealed that the mixture of dicalcium phosphate dihydrate (DCPD), $Ca(OH)_2$ and $Sr(OH)_2$ $8H_2O$ was phase-transformed into strontium-containing carbonate amorphous apatite by this simple and economical mechanochemical synthesis method.

1. Introduction

Hydroxyapatite (HAp) is a material used in bone grafts, bone repair and replacement in regenerative medicine [1]. It has a similar composition to the main inorganic component of bone and is an apatite that is indispensable to living organisms. The chemical formula of hydroxyapatite is $Ca_{10}(PO_4)_6(OH)_2$ [2]. The Ca^{2+} ions in the structure can be replaced by other metal ions such as Mg, Ag, Zn, Cu, Ti, Ba, Fe, and Sr [3]. It has been reported that strontium ions can affect bone remodeling by influencing both osteoclasts and osteoblasts [4]. Studies have been conducted on the release of strontium ions from biomaterials containing strontium [5]. In addition, it has been reported that these biomaterials can be used to treat osteoporosis, promote bone remineralization, suppress bone resorption, and maintain bone formation [5]. Strontium is also utilized in osteoporosis treatment drugs, such as strontium ranelate. Furthermore, it is known to improve osteoblast activity, which affects bone formation by matrix-mediated inhibition, and inhibits osteoclast differentiation to reduce bone resorption [6]. Luz et al. have reported that compared with Hap, strontium apatite is less toxic and shows a greater than 70% survival in the MC3T3 mouse cell line [7] as a bacterial cellulose membranes in the skull. Furthermore, Vukomanovic et al. synthesized an apatite containing strontium, magnesium, gallium, and zinc ions and demonstrated the synergistic effects of these ions in stimulating osteogenesis in human mesenchymal cells [8].

Mechanochemical synthesis, which involves grinding, agitation, and mixing of chemical compounds and solutions, promotes the chemical reactivity of raw materials to be thoroughly mixed based on their available high energy. Samples are subjected to repeated collisions with spinning balls or agitation. Due to compression and the associated deformation in an iterative process, the sample forms a submicron-sized crystal structure [9]. This mechanochemical grinding may result in a faster reaction rate than that of other normal grinding and reaction processes. By adjusting the weight of the prepared powder and the solutions added, we can achieve better control over the stoichiometry and operation system configuration. Chaikina et al. have reported the production of calcium phosphate via mechanochemical synthesis using a mixture of DCPD and CaO, which involved the use of a planetary ball mill operated at speeds of 1500 RPM for 30 min [10], whereas Makarova et al. have described substituted apatite containing zinc and silicon ions, which has been reported to have low toxicity and high viability [11].

* Corresponding author.
E-mail address: y.otsuka@dent.kagoshima-u.ac.jp (Y. Otsuka).

https://doi.org/10.1016/j.oceram.2023.100459
Received 24 May 2023; Received in revised form 11 August 2023; Accepted 6 September 2023
Available online 7 September 2023

Although a number of different nanoparticles were synthesized using this method, Macha et al. reported that apatite and, in general, calcium phosphate synthesized by mechanochemical synthesis can be easily produced using powders of calcium-based materials and phosphoric acid or ammonium dihydrate and ammonium dihydrogen phosphate, or simply by milling powders containing hydroxides and phosphates with each other [12]. Mochales et al. reported the mechanochemical synthesis of HAp from dicalcium phosphate dihydrate (DCPD) and calcium oxide [13]. Ito et al. reported a method for synthesizing chlorapatite and zinc-ion-substituted chlorapatite by mechanochemical synthesis using calcium chloride [14,15]. Bulina et al. have reported strontium- and magnesium-substituted apatite produced via mechanochemical synthesis [16], and the synthesis of strontium apatite from a mixture of $CaHPO_4$, CaO, and $SrCO_3$ has also been reported.

Terahertz (THz) spectroscopy is a useful tool for evaluating the polymorphism and quality of organic and inorganic crystals in various samples. The characterization of perovskite crystals has also been investigated [17]. THz can also characterize ceramic crystals; Ceramic $DyFeO_3$, which emits light in the THz band, has also been reported to exhibit magnetic changes [18]. The THz spectra of Class III ceramic tiles according to JIS A 5209:2014 revealed that the transmittance background varied depending on the firing temperature [19]. The cryogenic decomposition of zirconia bioceramics was also revealed using THz spectroscopy [20]. The use of THz spectroscopy for caries diagnosis was reported by Cai et al. [21]; thus we suggest that substituted apatite could be characterized using this novel technique.

In a previous study, we evaluated a tetracalcium phosphate and dicalcium phosphate mixture by infrared spectral analysis with a machine learning program called “principal component analysis” [22]. The mixture was transformed into HAp with a change in carbon dioxide concentration. This suggests that the concentration of carbon dioxide affects the growth of carbonate apatite. Chlorapatite containing zinc ions were prepared by mechanochemical synthesis and evaluated by FT-IR, XRD, and X-ray CT [15].

In this study, we report the development and evaluation of a simple and economical mechanochemical synthetic pathway to produce carbonate strontium apatite-based biomaterials. The mechanochemical synthesis method and characterization of the different amounts of strontium ions in apatite using FT-IR spectroscopy, X-ray diffraction, lattice constant measurements, THz spectroscopy, and morphology were investigated by SEM.

2. Materials and methods

2.1. Materials

DCPD, calcium hydroxide, and strontium hydroxide octahydrate were purchased from Fujifilm Wako Pure Chemical Corporation (Japan) as pure, raw chemical materials.

2.2. Procedure

2.2.1. Sample preparation

Powders were ground using a planetary ball milling machine (P6 classic line, Fritsch Japan Co., Ltd) that was applied to DCPD, strontium hydroxide octahydrate, and calcium hydroxide mixtures at different Sr/Sr+Ca molar ratios from 0% to 40.2%. The mixture of powder and water was ground at a powder-to-liquid ratio of 0.5. The samples were ground for 1 h at 500 RPM with 10 balls of 10 mm diameter in an 80 mL jar. The balls and jars were composed of alumina. The prepared samples were then incubated at 40 °C for more than 24 h.

2.3. X-ray diffraction

Diffractograms were obtained using an XRD diffractometer (PANalytical X’Pert PRO MPD, Malvern Panalytical Co.). The measurements were carried out under CuK_α radiation at 45 kV and 40 mA, with a minimum step size of 2 theta of 0.001°and in the range 2 theta = 5–40°. A loosely packed powder was prepared for testing in a glass holder.

2.3.1. Rietveld refinement

Rietveld refinement values based on XRD patterns were calculated using HighScore (Version 4.9; Malvern Panalytical B.V. 2020, UK).

2.4. Fourier-transform infrared spectroscopy

Infrared spectra of all samples were measured using a Fourier Transform Infrared (FTIR) spectrometer (FT/IR-4200, JASCO Co., Tokyo, Japan) equipped with an ATR accessory, which was inserted directly into the light beam. The IR spectra of the samples were measured in the range 500–4,000 cm^{-1} at a resolution of 1 cm^{-1}. Totalization was performed 64 times. The air spectrum was subtracted from the average spectrum to obtain the background.

2.5. Thermal analysis

The thermal stability was studied using thermogravimetric and differential thermal analyzer (TG-DTA; Rigau Co. Ltd, Themo plus evo TMA 8310, Japan) at temperatures ranging from 40 to 1000 °C at a heating rate of 10 °C/min.

2.6. Raman spectroscopy

Raman spectra were obtained using a laser Raman system (RAMAN basic PS-KU, Nanophoton Co., Japan). The measurement conditions were as follows: excitation wavelength of 532.00, laser current of 100%, and excitation power of 0.322122 mW, with ND filter 99.6%, and at center wavenumber of 1450, and total exposure time of 60 s.

2.7. Energy dispersive X-ray spectroscopy

Powder samples were pulverized in an agate mortar, and pellets with a diameter of 3 mm were produced using a lab compression sample hand tableting machine. After the preparation, the pressed samples were fixed to the specimen holder with carbon tape, and carbon coating was performed with a sputter coater. The samples were tested using SEM-EDS (SEM: FEI Quanta400, EDS: EDX Octane Elect Super). The accelerating voltage and magnification were 15.0 kV and X500 times.

2.8. Terahertz spectroscopy

We previously reported a device equipped with a light source and a cryostat based on differential frequency generation in a Gallium Phosphide (GaP) crystal [23,24]. The frequency range is from 0.6 THz to 6.0 THz. The sample was cooled at a constant temperature from 300 K to 70 K using liquid nitrogen during the sample stage. Absorbance was calculated from the difference between the sample and blank power spectra. The measurement sequence was controlled by a personal computer using proprietary software. The prepared apatite was directly compressed to prepare 10 wt% tablets diluted with polyethylene.

3. Results

3.1. Characterization of prepared apatite sample with XRDs

Fig. 1 shows the XRD patterns of pure (strontium-free) apatite and the prepared strontium apatite. Sample 0% was a milled mixture of DCPD and $Ca(OH)_2$ without strontium. The (211) peak was observed at 31.84°, which is thought to indicate the hexagonal crystals of carbonate apatite. In addition, peaks corresponding to the (210) and (022) planes were observed at 29.0° and 25.8, 2 theta degrees, further suggesting a hexagonal transition. Similar to our work, it has also been reported that

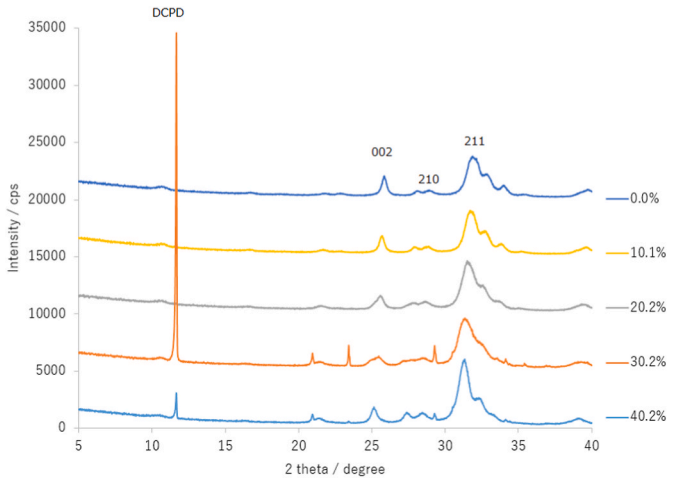

Fig. 1. PXRD patterns of strontium non-substituted apatite and strontium apatite.

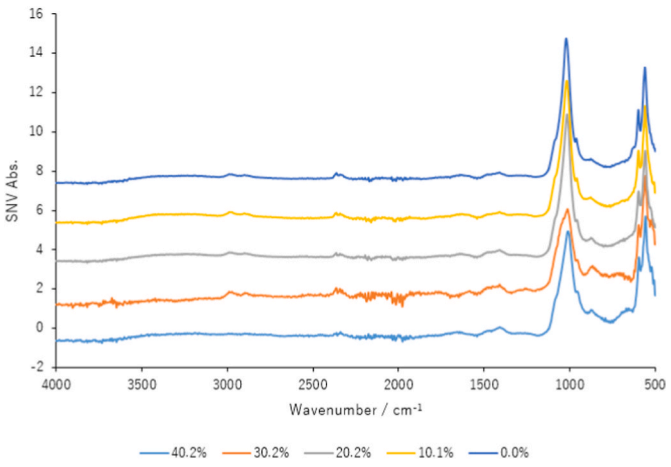

Fig. 2. FT-IR spectroscopy of prepared samples.

[8] carbonate apatite can be formed from DCPD and CaO mixtures. Samples with a Sr ratio between 10.1% and 40.2% contain strontium ions. The samples with Sr 40.2% and 30.2% showed a DCPD peak at 11.6, 2 theta degrees.

Rietveld refinement was applied to all XRD patterns. The Sr 40.2% sample comprised 15% DCPD (ICDD code: 00-011-0293) and 85% hydroxylapatite, strontian, syn [ICDD code: 01-075-8115: $(Sr_{2.27}Ca_{2.73})(PO_4)_3(OH)$]; the Sr 30.2% sample comprised 32% DCPD (ICDD code: 00-011-0293) and 68% hydroxylapatite, strontian, syn [ICDD code: 01-089-5632: $(Ca_{7.684}Sr_{2.316})(PO_4)_6(OH)_2$]; the Sr 20.2% sample was hydroxylapatite, strontian, syn [ICDD code: 01-077-9001: $(Ca_{8.542}Sr_{1.458})(PO_4)_6(OH)_2$]; the Sr 10.2% sample was hydroxylapatite, strontian, syn [ICDD code: 01-075-8114: $(Sr_{0.3}Ca_{4.7})(PO_4)_3(OH)$]; and the Sr 0% sample was hydroxylapatite [ICDD code: 01-074-0565: $Ca_{10}(PO_4)_6(OH)_2$]. The calculated apatite lattice parameter values are listed in Table .1. The lattice lengths a and c were found to increase with increasing strontium ion concentration, which can be attributed to the fact that the radii of calcium and strontium ions are 1.00 and 1.18 Å, respectively. This accordingly indicates that strontium ions are larger than those of calcium, thereby resulting in a larger crystal lattice.

3.2. FTIR analysis and Raman analysis

Fig. 2 shows the changes in the IR absorption spectra with Sr ion concentration prepared at different ratios. The spectrum of Sr 0% sample was characterized by prominent peaks at 1,020, 873, 598, and 556 cm^{-1}. The peak at 873 cm^{-1} is indicative of the presence of carbonate ions, and it is thus presumed that Sr 0% sample is a B-type carbonate apatite. Samples with values between 10.2% and 40.2% are also characterized by an apatite-specific peak at approximately 1,000 cm^{-1}. The peak at 873 cm^{-1} also indicates that similar to the Sr 0% sample, these samples also contain carbonate ions. Neither the phosphate vibrational peak of DCPD nor the sharp OH peak at 3,628 cm^{-1} for $Ca(OH)_2$ were found in samples containing Sr^{2+} ions.

Fig. 3 shows the Raman spectra of apatite. Raman spectroscopy is known to be effective for characterizing material. Apatite is known to exhibit a unique peak at 960 cm^{-1} [25]. In Fig. 3, all apatite samples containing strontium ions showed peaks at approximately 957 cm^{-1}. Fig. 3b shows the graph of the first derivative of the spectrum. It was revealed that the peak (band) point crossed 0, and the peak width changed depending on the strontium ion concentration. In this study, we attempted to quantitatively measure carbonate ions using TG.

Table 1
Lattice parameters of prepared samples apatite.

Sr/Sr+Ca	DCPD amount(%)	a (Å)	b (Å)
40.2%	15	9.590(2)	7.079(1)
30.2%	32	9.5721(7)	7.0422(6)
20.2%	0	9.519(3)	6.976(2)
10.1%	0	9.483(2)	6.939(2)
0%	0	9.446(3)	6.897(2)

3.3. Thermogravimetric analysis

The prepared samples were stored at 40 °C for up to 24 h. Subsequently, the samples were heated between 40 °C and 1,000 °C and analyzed using TGDTA. Weight loss was measured in samples with Sr = 40.2%, 30.2%, 20.2%, 10.1% and 0% where weight decreased by 9.93%, 8.72%, 7.05%, 8.08%, and 8.77% respectively from 40 °C to 400 °C.

Fig. 4 shows thermal analysis of the prepared samples. It was considered that this was due to the evaporation of free water and chemically bound water contained in the powders produced, as the wet synthesis was carried out with a water mixing ratio of 0.5. Tőnsuaadu et al. reported thermal analysis of various apatites with chemically bonded water [26]. The bound water evaporated and caused weight loss up to 400 °C, consistent with our results. Carbonation of carbonate ions contained around 700 °C is generally observed in the TGDTA measurement of apatite. In another report, Tőnsuaadu et al. investigated their TG-DTA analysis of complexed apatite containing calcium, ammonium, magnesium, phosphate, carbonate, fluoride and hydroxide ions [27]. The weight of carbonate ions contained in the change in weight between 600 °C and 900 °C is well known. Samples with Sr 40.2%, 30.2%, 20.2%, 10.1% and 0% showed a decrease of 0.65%, 0.96%, 0.29%, 0.02% and 0.16%, respectively from 600 °C to 900 °C. It was found that the carbonic acid content decreased as the proportion of strontium ions increased. This may be because the ionic radius of strontium ions is larger than that of calcium, resulting in a larger occupied volume. However, it was also reported that the carbonate ion is not completely absent. Spontaneous incorporation of carbonate ions was thought to be advantageous for crystal stabilization. Prabakaran et al. reported TG-DTA of apatite from the eggshell of hens [28]. They observed a weight loss from room temperature to 300 °C of 5.87%. The loss of carbonate ions between 700 °C and 850 °C was a small amount. Thermal analysis also revealed that all the apatite samples contained carbonate ions. It was indicated that carbonate ions would increase the biocompatibility of synthesized strontium apatite by adjusting the solubility. The Sr 30.2% sample was sinted at 1000 °C, the XRD pattern of which is shown in Fig. 1S, and is suggested to be HAp.

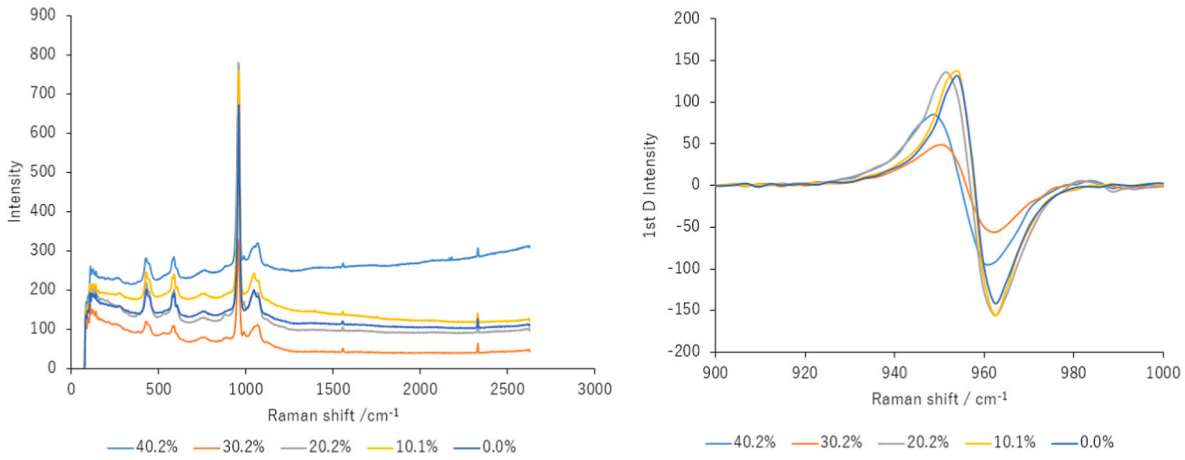

Fig. 3. Raman spectroscopy of prepared samples. (a) Raman raw spectra, (b) 1st derivative spectra.

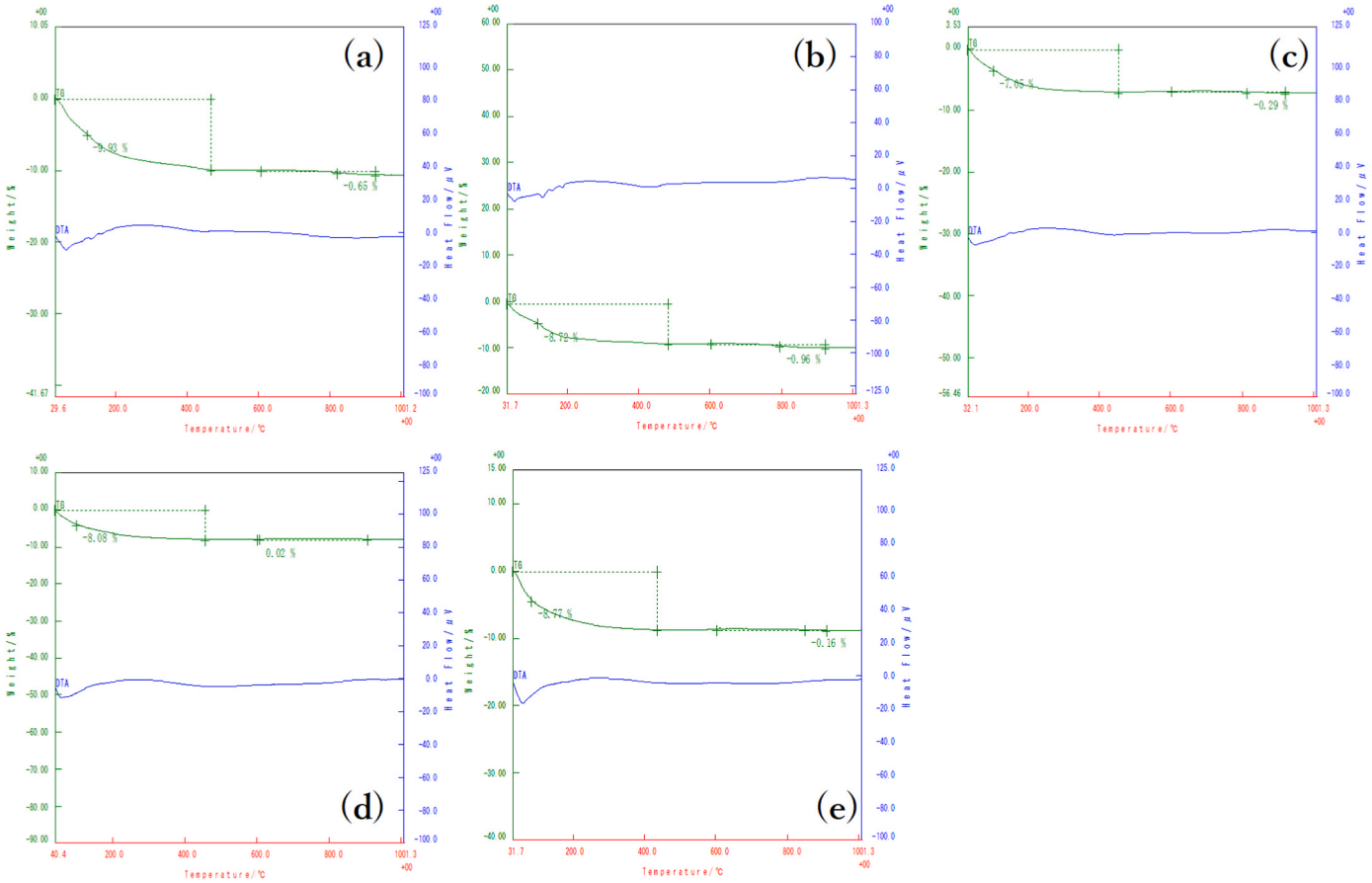

Fig. 4. TG/DTA analysis of prepared apatite samples. (a) 40.2%, (b) 30.2%, (c) 20.2%, (d) 10.1%, (e) 0%.

3.4. SEM and EDX analysis

Fig. 5 shows the results of EDX analysis for strontium substituted apatite. SEM images are shown in Fig. 2S. The Compression molded samples after grinding were analyzed by SEM-EDS spectrometry. The strontium-rich sample with Sr 40.2% showed the highest strontium peak. Samples containing strontium from Sr 40.2%–0% showed strontium compositions at 1.8 keV. Strontium was not detected in the HAp sample with Sr 0%. Carbon was detected in all samples, confirmed by a peak derived from carbon coating.

In this study, it is clear from the XRD patterns that the Sr 40.2% and Sr 30.2%, samples did not completely transform into strontium apatite and retained the composition of DCPD. Compressed particles were found in the samples with Sr 40.2% and Sr 30.2%. However, samples with Ca/P ratios of Sr 20.2%, Sr 10.1% and Sr 0% were found to have smooth surfaces.

3.5. Terahertz spectroscopy analysis

Fig. 6 shows the spectra of strontium-containing apatite at 70 K and 300 K. Absorption peaks were observed at 2.37 THz and 2.90 THz in Fig. 6a. The 2.37 THz peak is likely to be due to polyethylene, the

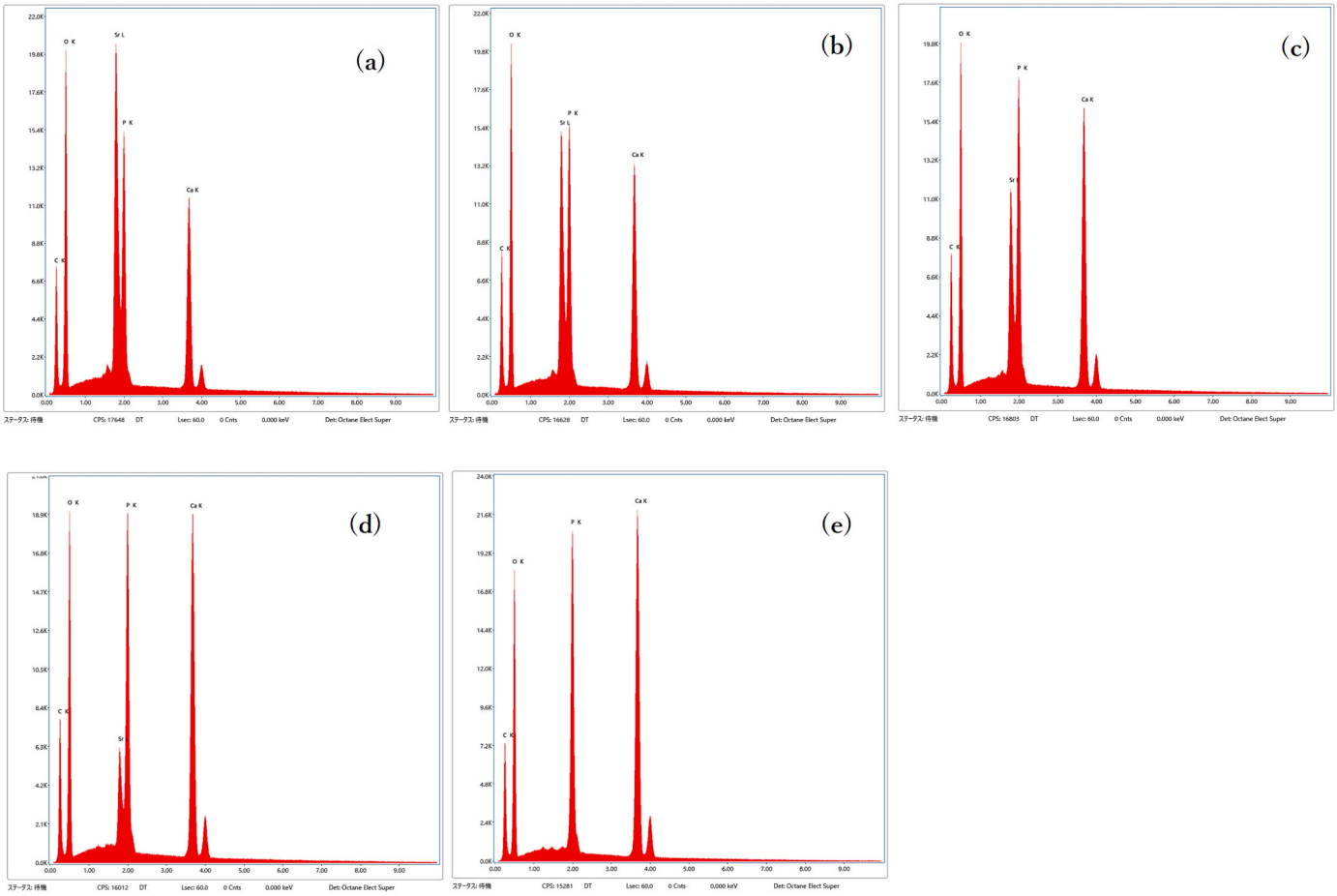

Fig. 5. EDX analysis of prepared apatite samples. (a) 40.2%, (b) 30.2%, (c) 20.2%, (d) 10.1%, (e) 0%.

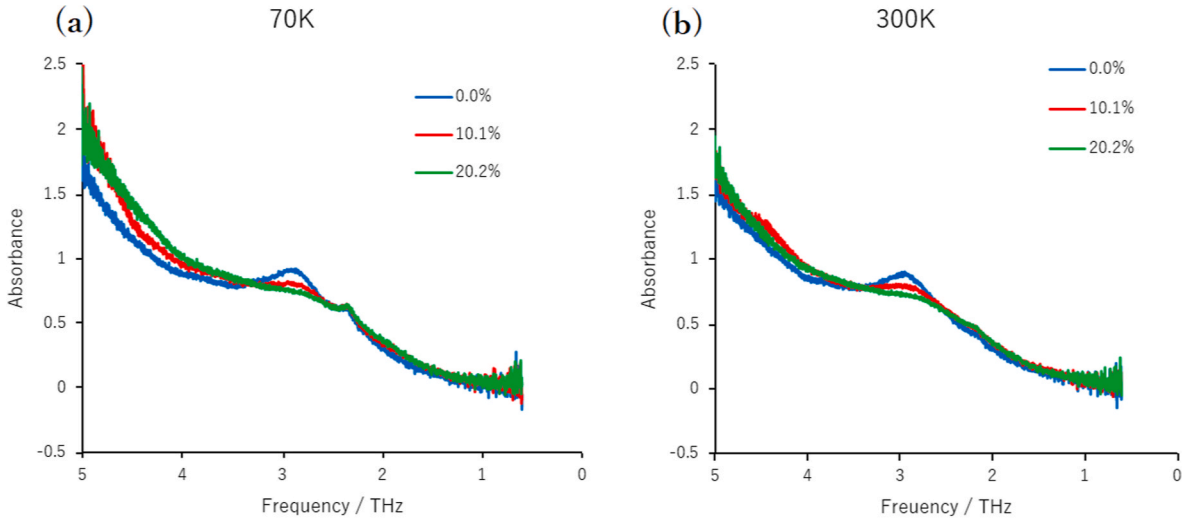

Fig. 6. Terahertz spectra of prepared apatite samples. (a) 70K (b) 300K.

diluent. It was found that the 2.9 THz spectrum disappeared with the increase in strontium ions. A difference in the baseline was observed from 4 to 5 THz. Further calculations, such as DFT, are required to determine the vibration mode, but the data indicate that THz is effective for characterization. Terahertz measurements at 300 K show a peak at 3 THz. It was suggested that the 70 K peak may have shifted because of temperature changes.

4. Discussion

In the future, the development of bioceramics will address the ever-increasing number of patients with osteoporosis. Notably, there are several types of bioceramics, of which apatite mimics a living body and exhibits high biocompatibility [29]. Studies have focused on the use of zirconia, perovskite, and other materials; however, apatite is a

biomaterial known for its bioreplaceability. Sintered, highly crystalline apatite has previously been used as a biomaterial, although recent studies have been conducted using octacalcium phosphate [30], which contains carbonic acid and is more amorphous. The difference between low crystallinity apatite and highly crystalline apatite is in bone resorption.

Functional and pharmacological apatite can be synthesized using various ions. Strontium ions are typical examples, and are known to suppress osteoclast differentiation [31]. We hypothesize that the synthesized low-crystalline strontium apatite has high bone resorption and releases strontium ions to suppress osteoclast differentiation.

It has been reported that differences in the peak widths in the Raman spectra indicate crystallinity. The strontium apatite sample with a sample of Sr 30.2% was low in crystallinity. At 1,070 cm^{-1}, it has been reported that the carbonate ν_1 mode and phosphate ν_3 mode are intricately intertwined [25]. The synthesized strontium carbonate apatite was considered to be a B-type structure. Careful analysis of this area is quantifiable.

The detection of strontium ions in crystals using conventional techniques, such as FT-IR, Raman, and TG-DTA has been ambiguous. Furthermore, XRD Rietveld refinement showed Sr ions; thus, we can assume that apatite contained Sr ions. We were able to characterize small differences based on crystal lattice sizes.

The FTIR spectra, together with the XRD results, revealed that the mixture of DCPD, $Ca(OH)_2$ and $Sr(OH)_2$ was phase-transformed into strontium-containing carbonate apatite by mechanochemical synthesis. The chemical reaction is proposed to be as follows:

$$6CaHPO_4 2H_2O + (4-x)Ca(OH)_2 + x\,Sr(OH)_2 8H_2O + y(CO_3^{2-})$$

$$\rightarrow (Ca_{1-x}Sr_x)_{10}(PO_4)_{6-\frac{2y}{3}}(CO_3)_y(OH)_2 + (12+8x)\,H_2O \qquad \text{Eq.1}$$

The apatite formed is considered to be a complex apatite composed of five components: calcium, strontium, phosphate, carbonate, and hydroxyl ions. Ren et al. reported [32] that infrared spectroscopy of the carbonate ions in carbonated apatite produced peaks at 876 cm^{-1} and 1, 419 cm^{-1}, which is in agreement with the present study. In another report [33], carbonate ions in bone minerals were identified. In this study, carbonated ion peaks were observed in the bone, and the number of carbonated ions increased with age and maturation. Yoder et al. reported [34] the infrared spectra of carbonated strontium apatite. Carbonated ion vibrations were observed from 1,400 to 1,500 cm^{-1}. Many studies have shown that carbonate ions are incorporated during apatite synthesis. It is conceivable that this occurs not only with strontium ions, but also with other substitutional ions.

Terahertz spectroscopy is a relatively new spectroscopic method. Terahertz waves are electromagnetic waves ranging from far-infrared to millimeter waves, with frequencies between 0.1 and 10 THz. It is characterized by the unique permeability of electromagnetic waves and the ability to obtain spectra unique to specific substances. It is used in a wide range of applications such as the separation of crystal polymorphs in pharmaceuticals, evaluation of industrial products, and quality control in manufacturing processes.

Yatongchai et al. reported [35] a THz spectra of HAp at 1.2 THz using terahertz time-domain Spectroscopy (THz-TDS). In this study, we did not observe this peak as we focused on the range of 2 THz to 5 THz. Plazanet et al. reported [36] a 2.1 THz peak for HAp using TDS. A few peaks were evident in the same range at 300 K; however, the baseline variation was greater and less detailed. It became clear that characterization was possible using the THz spectrum. This technique can also be used for measurements at low temperatures, thus, enabling evaluation of the phase transition in a cryogenic state. These techniques can be applied to the development of quantum computer materials, superconducting materials, and the consideration of the phase transition and behavior of ceramics at extremely low temperatures in the outer space. The results of THz spectroscopy showed a prominent peak, indicating that characterization is possible, which reinforces the effectiveness and use of THz spectroscopy in the future development of low-crystallinity ceramics.

5. Conclusions

The FT-IR spectra, in combination with the XRD results, revealed that the mixture of DCPD, $Ca(OH)_2$ and $Sr(OH)_2$ $8H_2O$ was phase-transformed into strontium-containing carbonate apatite by mechanochemical synthesis. However, retained raw materials were also detected, indicating that the transformation was not complete during the time period used. XRD and TG-DTA results revealed the presence of carbonate ions. Carbonate contamination in wet mechanochemical synthesis is caused by carbonate ions in the solution. Strontium carbonate apatite is a bioceramic material that can be applied as a bone graft and filling material. The mechanochemical method used in this study is provides simple and economical formation and synthesis of substituted apatite. It also became clear that the characterization of apatite-based ceramics is possible using THz spectroscopy.

Funding statement

A part of this research is based on the Cooperative Research Project of Research Center for Biomedical Engineering. This research was partialy supported by KAKENHI Grant Number 23K16044.

Declaration of competing interest

The authors declare that they have no known competing financial interests or personal relationships that could have appeared to influence the work reported in this paper.

Acknowledgements

The authors would like to thank Mr. Shingo Kubo and Mr. Hirokazu Ohkura, Division of Instrumental Analysis, Center for Advanced Science Research and Promotion, Kagoshima University for their valuable comments and technical support.

Appendix A. Supplementary data

Supplementary data to this article can be found online at https://doi.org/10.1016/j.oceram.2023.100459.

References

[1] K. Pajor, L. Pajchel, J. Kolmas, Hydroxyapatite and fluorapatite in conservative dentistry and oral implantology—a review, Materials 12 (2019), https://doi.org/10.3390/ma12172683.
[2] S. Hu, F. Jia, C. Marinescu, F. Cimpoesu, Y. Qi, Y. Tao, A. Stroppa, W. Ren, Ferroelectric polarization of hydroxyapatite from density functional theory, RSC Adv. 7 (2017) 21375–21379.
[3] M. Wang, Q. Wang, X. Lu, K. Wang, F. Ren, Computer simulation of ions doped hydroxyapatite: a brief review, J. Wuhan Univ. Technol.-Materials Sci. Ed. 32 (2017) 978–987.
[4] C.R. Scardueli, C. Bizelli-Silveira, R.A.C. Marcantonio, E. Marcantonio, A. Stavropoulos, R. Spin-Neto, Systemic administration of strontium ranelate to enhance the osseointegration of implants: systematic review of animal studies, Int. J. Implant Dent. 4 (2018) 1–9.
[5] N. Neves, D. Linhares, G. Costa, C. Ribeiro, M. Barbosa, In vivo and clinical application of strontium-enriched biomaterials for bone regeneration: a systematic review, Bone & Joint Research 6 (2017) 366–375.
[6] J. Reginster, Strontium ranelate in osteoporosis, Curr. Pharmaceut. Des. 8 (2002) 1907–1916.
[7] E.P.C.G. Luz, A.L. de Brito Soares, F.F.P. de Souza, F.K. Andrade, I.I. Castro-Silva, M. de Freitas Rosa, R.S. Vieira, Implantable matrixes of bacterial cellulose and strontium apatite: preclinical analysis of cytotoxicity and osteoconductivity, Mater. Today Commun. 33 (2022), 104871.
[8] M. Vukomanovic, L. Gazvoda, N. Anicic, M. Rubert, D. Suvorov, R. Müller, S. Hofmann, Multi-doped apatite: strontium, magnesium, gallium and zinc ions synergistically affect osteogenic stimulation in human mesenchymal cells important for bone tissue engineering, Biomater. Adv. 140 (2022), 213051.

[9] R.-N. Rosa Cegla, I.J. Macha, B. Ben-Nissan, D. Grossin, G. Heness, R.-J. Chung, Comparative study of conversion of coral with ammonium dihydrogen phosphate and orthophosphoric acid to produce calcium phosphates, Journal of the Australian Ceramics Society 50 (2014) 154–161.
[10] M.V. Chaikina, N.V. Bulina, O.B. Vinokurova, K.B. Gerasimov, I.Y. Prosanov, N. B. Kompankov, O.B. Lapina, E.S. Papulovskiy, A.V. Ishchenko, S.V. Makarova, Possibilities of mechanochemical synthesis of apatites with different Ca/P ratios, Ceramics 5 (2022) 404–422.
[11] S.V. Makarova, N.V. Bulina, Y.A. Golubeva, L.S. Klyushova, N.B. Dumchenko, S. S. Shatskaya, A.V. Ishchenko, M.V. Khvostov, D.V. Dudina, Hydroxyapatite double substituted with zinc and silicate ions: possibility of mechanochemical synthesis and in vitro properties, Materials 16 (2023) 1385.
[12] I.J. Macha, I. Karacan, B. Ben-Nissan, S. Cazalbou, W.H. Müller, Development of antimicrobial composite coatings for drug release in dental, orthopaedic and neural prostheses applications, SN Appl. Sci. 1 (2019) 1–10.
[13] C. Mochales, H. El Briak-BenAbdeslam, M.P. Ginebra, A. Terol, J.A. Planell, P. Boudeville, Dry mechanochemical synthesis of hydroxyapatites from DCPD and CaO: influence of instrumental parameters on the reaction kinetics, Biomaterials 25 (2004) 1151–1158.
[14] A. Ito, Y. Otsuka, M. Takeuchi, H. Tanaka, Mechanochemical synthesis of chloroapatite and its characterization by powder X-ray diffractometory and attenuated total reflection-infrared spectroscopy, Colloid Polym. Sci. 295 (2017) 2011–2018.
[15] A. Ito, Y. Otsuka, M. Takeuchi, H. Tanaka, Mechanochemical synthesis of zinc chloroapatite and evaluation of its crystallinity by attenuated total reflection-infrared spectroscopy and principal component analysis, Phosphorus Res. Bulletin 35 (2019) 16–22.
[16] N.V. Bulina, O.B. Vinokurova, I.Y. Prosanov, A.M. Vorobyev, K.B. Gerasimov, I. A. Borodulina, A. Pryadko, V.V. Botvin, M.A. Surmeneva, R.A. Surmenev, Mechanochemical synthesis of strontium-and magnesium-substituted and cosubstituted hydroxyapatite powders for a variety of biomedical applications, Ceram. Int. 48 (2022) 35217–35226.
[17] F. Zhang, I. Karimata, H.-W. Wang, T. Tachikawa, K. Tominaga, M. Hayashi, T. Sasaki, Terahertz spectroscopic measurements and solid-state density functional calculations on CH3NH3PbBr3 perovskites: short-range order of methylammonium, J. Phys. Chem. C 126 (2021) 339–348.
[18] X. Fu, X. Liu, J. Zhou, Terahertz spectroscopic observation of spin reorientation induced antiferromagnetic mode softening in DyFeO3 ceramics, Mater. Lett. 132 (2014) 190–192.
[19] S. Niijima, M. Shoyama, K. Kawase, Nondestructive inspection of sinterability of ceramic tiles by terahertz spectroscopy, Electron. Commun. Jpn. 102 (2019) 19–24.
[20] S. Ahmed, M. Zhang, V. Koval, L. Zou, Z. Shen, R. Chen, B. Yang, H. Yan, Terahertz probing of low-temperature degradation in zirconia bioceramics, J. Am. Ceram. Soc. 105 (2022) 1106–1115.
[21] J. Cai, M. Guang, J. Zhou, Y. Qu, H. Xu, Y. Sun, H. Xiong, S. Liu, X. Chen, J. Jin, Dental caries diagnosis using terahertz spectroscopy and birefringence, Opt Express 30 (2022) 13134–13147.
[22] Y. Otsuka, M. Takeuchi, M. Otsuka, B. Ben-Nissan, D. Grossin, H. Tanaka, Effect of carbon dioxide on self-setting apatite cement formation from tetracalcium phosphate and dicalcium phosphate dihydrate; ATR-IR and chemoinformatics analysis, Colloid Polym. Sci. 293 (2015) 2781–2788, https://doi.org/10.1007/s00396-015-3616-6.
[23] T. Sasaki, T. Sakamoto, M. Otsuka, Detection of impurities in organic crystals by high-accuracy terahertz absorption spectroscopy, Anal. Chem. 90 (2018) 1677–1682.
[24] Y. Otsuka, A. Ito, M. Takeuchi, T. Sasaki, H. Tanaka, Effects of temperature on terahertz spectra of caffeine/oxalic acid 2: 1 cocrystal and its solid-state density functional theory, J. Drug Deliv. Sci. Technol. (2019), 101215.
[25] A. Awonusi, M.D. Morris, M.M. Tecklenburg, Carbonate assignment and calibration in the Raman spectrum of apatite, Calcif. Tissue Int. 81 (2007) 46–52.
[26] K. Tõnsuaadu, M. Peld, V. Bender, Thermal analysis of apatite structure, J. Therm. Anal. Calorim. 72 (2003) 363–371.
[27] K. Tonsuaadu, K.A. Gross, L. Plüduma, M. Veiderma, A review on the thermal stability of calcium apatites, J. Therm. Anal. Calorim. 110 (2012) 647–659.
[28] K. Prabakaran, A. Balamurugan, S. Rajeswari, Development of calcium phosphate based apatite from hen's eggshell, Bull. Mater. Sci. 28 (2005) 115–119.
[29] Y. Otsuka, Synthesis of hydroxyapatite: crystal growth mechanism and its relevance in drug delivery applications, in: A.H. Choi, B. Ben-Nissan (Eds.), Innovative Bioceramics in Translational Medicine I: Fundamental Research, Springer Singapore, Singapore, 2022, pp. 213–229, https://doi.org/10.1007/978-981-16-7435-8_7.
[30] S. Barinov, V. Komlev, Osteoinductive ceramic materials for bone tissue restoration: octacalcium phosphate, Inorganic Materials, Appl. Res. 1 (2010) 175–181.
[31] Q. Wu, L. Hu, R. Yan, J. Shi, H. Gu, Y. Deng, R. Jiang, J. Wen, X. Jiang, Strontium-incorporated bioceramic scaffolds for enhanced osteoporosis bone regeneration, Bone Res. 10 (2022) 55, https://doi.org/10.1038/s41413-022-00224-x.
[32] F. Ren, Y. Ding, Y. Leng, Infrared spectroscopic characterization of carbonated apatite: a combined experimental and computational study, J. Biomed. Mater. Res. Part A: An Official Journal of The Society for Biomaterials 102 (2014) 496–505. The Japanese Society for Biomaterials, and The Australian Society for Biomaterials and the Korean Society for Biomaterials.
[33] C. Rey, V. Renugopalakrishman, B. Collins, M.J. Glimcher, Fourier transform infrared spectroscopic study of the carbonate ions in bone mineral during aging, Calcif. Tissue Int. 49 (1991) 251–258, https://doi.org/10.1007/BF02556214.
[34] C.H. Yoder, X. Lyu, The carbonate location in mixed calcium and strontium carbonated apatites, Polyhedron 179 (2020), 114365, https://doi.org/10.1016/j.poly.2020.114365.
[35] C. Yatongchai, A. Wren, S. Sundaram, Characterization of hydroxyapatite-glass composites using terahertz time-domain spectroscopy, J. Infrared, Millim. Terahertz Waves 36 (2015) 81–93.
[36] M. Plazanet, J. Tasseva, P. Bartolini, A. Taschin, R. Torre, C. Combes, C. Rey, A. Di Michele, M. Verezhak, A. Gourrier, Time-domain THz spectroscopy of the characteristics of hydroxyapatite provides a signature of heating in bone tissue, PLoS One 13 (2018), e0201745.